Investigation of the Adjoint Method in Aerodynamic Optimization Using Various Shape Parameterization Techniques

Ebrahim Sharifi Tashnizi
Dr.sharifi@taut.ac.ir
Tafresh University
Dep. of Industrial and Mechanical Engineering
Tafresh, Iran

Azadeh Akhavan Taheri
A.AkhavanTaheriBorojeni@student.tudelft.nll
TU Delft University
Faculty of Mechanical, Maritime and Materials Engineering
Delft, Netherlands

Mohamad Hamed Hekmat
Mhamed_hekmat@yahoo.com
K. N. Toosi University of Technology
Department of Mechanical Engineering
Tehran, Iran

This paper studies the effect of design variables vector on automatic aerodynamic shape optimization in the adjoint method. Three shape techniques are studied: surface points, relations of the NACA 4-digit airfoil series and Hicks-Henne "Bump" Functions. First, this paper presents the complete formulation of the optimal design problem for the Euler equations. Second, the implementation of these surface representation methods are explored. Finally, results are presented for inverse and drag minimization problems. The results show that the mechanism, value and the trend of drag reduction during the optimization strongly affected by the type of design vector.
Keywords*: adjoint equations, shape optimization, Euler equations, design variables vector*

Introduction

Engineers continually strive to improve their designs to increase both their operational effectiveness and their market appeal. In the design of a complex engineering system, relatively small design changes can sometimes lead to significant benefits. For example, small changes in wing section shapes can lead to large reduction in shock strength in transonic flow. Changes of this type are unlikely to be discovered by trial and error methods, and for such situations that optimization methods can play an important role.

In the past, for a suitable design that provides a desired aerodynamic performance, designers needed to build numerous models for wind tunnel testing to confirm the final design performance. Such a design process does not allow for vast numbers of design iterations or variables to be considered. The development of computational fluid dynamics during recent decades has made possible to evaluate alternative designs by numerical simulation. The use of computational simulation to scan many alternative designs has proved extremely valuable in practice, but it still suffers the limitation of finding the best possible design. To ensure the recognition of the true best design, the ultimate goal of computational simulation methods should not just be the analysis of prescribed shapes, but automatic determination of the true optimum shape for the desired application. This is the underlying motivation for the combination of computational fluid dynamics with numerical optimization methods.

The adjoint method is one of a gradient-based method, which has been used extensively in many aerodynamic optimization problems in recent decades. Studies of using of the adjoint approach for optimum shape design of systems governed by elliptic equations were initiated by Pironneau (1984). The adjoint equations approach to optimal aerodynamic design was first applied to transonic flow by Jameson (1988, 1996 and 1997). He formulated the method for inviscid compressible flows with shock waves governed by both the potential flow and the Euler equations (1988). Elliot and Peraire (1997) used the discrete adjoint method on unstructured meshes for the inverse design of airfoils and in transonic flow to produce specified pressure distributions. In (2000), Dadone and Grossman explored the discrete adjoint method and applied it in the progressive optimization strategy. A comparison of both continuous and discrete adjoint approaches was conducted by Nadarajah and Jameson (2000, 2001 and 2003). Baysal and Ghayour (2001) derived the adjoint equations in Cartesian coordinates on an unstructured grid system using Roe's schemes. Vitturia and Beuxb (2006) implement the discrete adjoint approach for aerodynamic optimization in turbulent viscous flow. The adjoint method has also been used by many researchers in aerodynamic optimization including Xie (2002), Qiao et al. (2002), Gauger and Brezillon (2002), Dwight and Brezillon (2006), Amoignon (2004) and Hazra (2004).

The objective of the present paper is to implement the adjoint approach for airfoils optimization in inverse pressure design and constrained drag minimization problems. First, an inverse design problem is solved to evaluate the optimization algorithm. Second, in the drag minimization problem, the optimization is performed in a fixed lift coefficient and angle of attack is applied as an additional design variable to fix lift during the design process. To evaluate the performance of the adjoint method in design problems with numerous design variables and also to evaluate the effects of the adoption of the design vector on the optimization results, the constrained drag minimization is performed using two different design vectors. It was shown that the mechanism, value and the trend of drag reduction during the optimization was strongly affected by the type of design vector.

Nomenclature

- A = *jacobian matrix in physical domain*
- B = *boundary*
- c = *chord length*
- C = *inviscid jacobian matrixes, coefficient*
- D = *flow field domain*
- E = *total energy*
- f = *inviscid flux vector in physical domain, Hicks and Henne sine "bump" functions*
- F = *inviscid flux vector in computational domain, design variables vector*

Paper accepted October, 2009. Technical Editor: Francisco Ricardo Cunha

G = *gradient vector of cost function*
$\|G\|$ = *norm of gradient vector*
h = *step size*
H = *total enthalpy*
m = *step sizes in finite difference method*
I = *cost function*
J = *determinant of mapping derivatives*
K = *mapping derivatives matrix*
l = *grid line counter*
m = *maximum mean camber of the airfoil, number of step sizes*
M = *mach number*
N = *number of design variables*
n = *components of unit vector normal to the surface, design step counter*
O = *truncation error*
p = *chordwise position of the maximum mean camber, pressure*
R = *residual term of governing equation*
s = *surface element*
t = *maximum thickness of the airfoil, time*
T = *Temperature*
t_1 = *location of the maximum point of the bump*
t_2 = *controller parameter of the width of the bump*
u = *velocity component in physical domain*
U = *velocity component in computational domain*
w = *flow field variables in physical domain*
W = *flow field variables in computational domain*
x = *design variables vector, physical coordinates*
y_{basis} = *y component of initial surface point*
y_c = *camber line function*
y_t = *thickness function*

Greek Symbols

γ = *ratio of specific heats*
λ = *adjoint boundary condition parameter*
ρ = *density*
ε = *smoothing parameter*
ξ = *computational coordinates*
δ = *kronecker delta function, variation*
θ = *camber line slope*
α = *angle of Attack, step length in optimization algorithm*
ψ = *adjoint variable*
∇ = *gradient function*
$\overline{\nabla}$ = *smoothed gradient function*
∂ = *partial derivation*

Subscripts

b relative to wall
d relative to desired pressure, relative to drag
i counter
j counter
l relative to variable on the lower surface, relative to lift
p relative to pressure
u relative to variable on the upper surface
ξ relative to computational domain
I relative to contribution due to variation of the flow field variable
II relative to contribution due to variation of the design variable
n relative to present optimization step
$n+1$ relative to new optimization step
new relative to variable in present design cycle
old relative to variable in previous design cycle
1 relative to the first component
2 relative to the second component

General Description of the Adjoint Approach

For flow over an airfoil or wing, the aerodynamic properties, which define the cost function (I), are dependent to the flow field variables (w) and the physical location of the boundary (F):

$$I = I(w,F) \tag{1}$$

Since w depends on F, a change in F changes the cost function as:

$$\delta I = \left[\frac{\partial I^T}{\partial w}\right]_I \delta w + \left[\frac{\partial I^T}{\partial F}\right]_{II} \delta F \tag{2}$$

The first term is the contribution due to the variation δw in the flow field and the second term is the direct effect of the geometry change. Assume R is the governing equation, which expresses the relation of w and F in the flow field domain D:

$$R\,(w,F)=0 \tag{3}$$

Then δR is determined from the equation:

$$\delta R=\left[\frac{\partial R}{\partial w}\right]_I \delta w+\left[\frac{\partial R}{\partial F}\right]_{II} \delta F=0 \tag{4}$$

Since the variation δR is zero, it can be multiplied by a Lagrange Multiplier ψ and subtracted from the variation δI with no changing in the result. Thus Eq. (2) can be replaced by:

$$\delta I=\left\{\frac{\partial I}{\partial w}^T -\psi^T\left[\frac{\partial R}{\partial w}\right]\right\}_I \delta w+\left\{\frac{\partial I}{\partial F}^T -\psi^T\left[\frac{\partial R}{\partial F}\right]\right\}_{II} \delta F \tag{5}$$

In order to eliminate the dependence of δI to δw, ψ must satisfy the adjoint equations:

$$\left[\frac{\partial R}{\partial w}\right]^T \psi=\frac{\partial I}{\partial w} \tag{6}$$

The first term is eliminated, and we find that:

$$\delta I = G\,\delta F \tag{7}$$

where

$$G=\frac{\partial I}{\partial F}^T -\psi^T\left[\frac{\partial R}{\partial F}\right] \tag{8}$$

According to Eq. (7) and Eq. (8), δI is independent of δw and, as a result, for a large number of design variables, we can compute the gradient vector (G) only with one flow solution in addition to one adjoint solution in each design cycle. It should be noted that the computational cost of one adjoint solution is less than one flow solution. After calculating the gradient vector, we can improve the design variables using an optimization algorithm.

Governing Equations

In this study the Euler equations are the governing equations of the field. The conservative form of two-dimensional Euler equations is as:

$$\frac{\partial w}{\partial t}+\frac{\partial f_i}{\partial x_i}=0 \tag{9}$$

where w is flow variables and f_i is the inviscid flux vector:

$$w=\begin{bmatrix}\rho\\ \rho u_1\\ \rho u_2\\ \rho E\end{bmatrix},\ f_i=\begin{bmatrix}\rho u_i\\ \rho u_i u_1+\delta_{i1}p\\ \rho u_i u_2+\delta_{i2}p\\ \rho u_i H\end{bmatrix} \tag{10}$$

and δ_{ij} is the Kronecker delta function and:

$$p=(\gamma-1)\rho\left\{E-\frac{1}{2}(u_i^{\,2})\right\} \tag{11}$$

$$\rho H=\rho E+p \tag{12}$$

In these definitions, ρ is the density, E is total energy, H is total enthalpy and γ is the ratio of specific heats. Using a transformation from physical coordinates to computational coordinates, the Euler equations can be written as:

$$\frac{\partial W}{\partial t}+R(W)=0 \tag{13}$$

where

$$R(W)=\frac{\partial F_i}{\partial \xi_i},\ W=Jw,\ F_i=S_{ij}f_j=\begin{bmatrix}\rho U_i\\ \rho U_i u_1+S_{i1}p\\ \rho U_i u_2+S_{i2}p\\ \rho U_i H\end{bmatrix} \tag{14}$$

$$K_{ij}=\left[\frac{\partial x_i}{\partial \xi_j}\right],\ J=\det(K),\ S=JK^{-1} \tag{15}$$

The scaled contravariant velocity components are introduced as:

$$U_i=S_{ij}u_j \tag{16}$$

In the computational domain, airfoil surface B_W is presented by $\xi_2=0$. The boundary condition on the airfoil surface is:

$$U_2=0\ \ On\ B_W \tag{17}$$

On the far field boundary, the free stream condition is applied.

A finite-volume technique with an artificial dissipation method introduced by Jameson, Schmidt and Turkel (1981) is used to discrete the integral form of the conservation equations. For temporal approximation, we applied the five stage modified Runge-Kutta approach. Since the time step in explicit methods is small, we applied the convergence acceleration techniques, local time stepping and residual averaging, to accelerate the convergence rate.

Adjoint Equations

In this section, we drive the adjoint equations and its boundary conditions for inverse design problem.

The design problem can be studied as a control problem choosing airfoil surface as the control function to minimize the cost function I subject to constraints defined by the flow equations. The cost function for inverse design problem is defined as:

$$I=\frac{1}{2}\int_{Bw}(p-p_d)^2 ds \tag{18}$$

or in the computational domain

$$I=\frac{1}{2}\int_{Bw}(p-p_d)^2\,|ds|d\xi \tag{19}$$

where

$$|ds|=(S_{2j}\,S_{2j})^{1/2} \tag{20}$$

p_d is the desired pressure on the surface. A variation in the shape results in a variation δI in the cost function:

$$\delta I=\int_{Bw}(p-p_d)\delta p\,ds+\frac{1}{2}\int_{Bw}(p-p_d)^2\,\delta ds \tag{21}$$

From Euler equations in the steady state:

$$\frac{\partial}{\partial \xi_i}\delta F_i=0 \tag{22}$$

where

$$\delta F_i=C_i\,\delta w+\delta S_{ij}f_j \tag{23}$$

$$C_i=S_{ij}A_j\ \ ,\ \ A_j=\frac{\partial f_j}{\partial w} \tag{24}$$

Multiplying Eq. (22) by a co-state variable vector, ψ and integrating over the domain, we have:

$$\int_D \psi^T\frac{\partial \delta F_i}{\partial \xi_i}dD_\xi=0 \tag{25}$$

Assuming ψ is differentiable and integrating by parts gives:

$$\int_B n_i\psi^T\,\delta F_i\ dB_\xi-\int_D\frac{\partial \psi^T}{\partial \xi_i}\delta F_i\ dD_\xi=0 \tag{26}$$

where n_i are the components of the unit vector normal to the surface in computational domain. Adding Eq. (26) to the variation of cost function, we have:

$$\begin{aligned}\delta I=&\int_{Bw}(p-p_d)\delta p\,ds+\frac{1}{2}\int_{Bw}(p-p_d)^2\,\delta ds-\\ &\int_D\frac{\partial \psi^T}{\partial \xi_i}\,\delta F_i dD+\int_B(n_i\psi^T\delta F_i)dB\end{aligned} \tag{27}$$

where

$$dD=d\xi\,d\eta\ ,\ dB=d\xi \tag{28}$$

From the third integral of Eq. (27), to eliminate the term, which contains δw, the adjoint equations can be obtained:

$$\frac{\partial \psi}{\partial t}-C_i^T\frac{\partial \psi}{\partial \xi_i}=0 \tag{29}$$

where ψ is adjoint variables vector. From flow boundary condition on the surface (Eq. (17)):

$$\delta F_2 = \delta p \begin{bmatrix} 0 \\ S_{21} \\ S_{22} \\ 0 \end{bmatrix} + p \begin{bmatrix} 0 \\ \delta S_{21} \\ \delta S_{22} \\ 0 \end{bmatrix} \tag{30}$$

The first and fourth integral in Eq. (27) with the above equation follows the adjoint boundary condition on the surface:

$$\psi_2 n_1 + \psi_3 n_2 = p - p_d \tag{31}$$

where n_1 and n_2 are the components of unit vector normal to the surface:

$$n_j = \frac{S_{2j}}{(S_{2j} S_{2j})^{1/2}} \tag{32}$$

But for better convergence and easier implementation, the adjoint boundary conditions on the surface can be derived as follow:

$$\begin{aligned} \psi_{1_{i,1}} &= \psi_{1_{i,2}} \\ \psi_{2_{i,1}} &= \psi_{2_{i,2}} + 2n_1 (\lambda - n_1 \psi_{2_{i,2}} - n_2 \psi_{3_{i,2}}) \\ \psi_{3_{i,1}} &= \psi_{3_{i,2}} + 2n_2 (\lambda - n_1 \psi_{2_{i,2}} - n_2 \psi_{3_{i,2}}) \\ \psi_{4_{i,1}} &= \psi_{4_{i,2}} \end{aligned} \tag{33}$$

where

$$\lambda = p - p_d \tag{34}$$

The subscripts (i,1) and (i,2) in the above equations denote cells below and above the wall. On the far field, with attention to fourth integral in Eq. (27), we must choose the ψ such that

$$n_i \psi^T C_i = 0 \tag{35}$$

For subsonic and transonic flows that the outer boundary is far from the body, we can set:

$$\psi_{1-4} = 0 \tag{36}$$

Because of the similarity of the adjoint equations to flow equations, the same numerical methods used to solve the flow equations can be used to solve the adjoint equations. This greatly simplified the procedure to implement the adjoint module. If the coordinate transformation is such that δS_{21} δS_{22} and are negligible in the far field, then the final expression for δI can be written as:

$$\begin{aligned} \delta I = \frac{1}{2} \int_{Bw} (p - p_d)^2 \, \delta |ds| d\xi - \int_D \frac{\partial \psi^T}{\partial \xi_i} \delta S_{ij} f_j \, d\xi \, d\eta - \\ \int_{Bw} (\delta S_{21} \psi_2 + \delta S_{22} \psi_3) \, p d\xi \end{aligned} \tag{37}$$

Constrained Optimization

In the drag minimization problem, we want to maintain the lift coefficient constant and equal to its initial value by changing the angle of attack. Therefore, in this case:

$$\delta I = \delta C_d = \frac{\partial C_d}{\partial w} \delta w + \frac{\partial C_d}{\partial F} \delta F + \frac{\partial C_d}{\partial \alpha} \delta \alpha \tag{38}$$

and the additional constraint is:

$$\delta C_l = \frac{\partial C_l}{\partial w} \delta w + \frac{\partial C_l}{\partial F} \delta F + \frac{\partial C_l}{\partial \alpha} \delta \alpha = 0 \tag{39}$$

or

$$\delta \alpha = - \frac{\frac{\partial C_l}{\partial w} \delta w + \frac{\partial C_l}{\partial F} \delta F}{\frac{\partial C_l}{\partial \alpha}} \tag{40}$$

The angle of attack is updated using Eq. (40) in each design cycle. To compute $\delta \alpha$ we need to solve an additional adjoint equation. The derivation process of adjoint equations and its boundary conditions for the constrained drag minimization is similar to the inverse design problem. For the drag minimization problem, Eq. (33) can be used to apply adjoint boundary condition on the surface. For the drag minimization problem, λ in Eq. (33) is:

$$\begin{aligned} \lambda = \frac{-2}{\gamma p_\infty M_\infty^2 c} [\; & (n_1 \cos \alpha + n_2 \sin \alpha) + \\ & \Phi (n_2 \cos \alpha - n_1 \sin \alpha) \;] \end{aligned} \tag{41}$$

$$\Phi = - \frac{\frac{\partial C_d}{\partial \alpha}}{\frac{\partial C_l}{\partial \alpha}} \tag{42}$$

where p_∞ and M_∞ are the free stream pressure and Mach number, c is chord length, γ is ratio of specific heats, α is angle of attack and C_l is lift coefficient.

Optimization Algorithm

In this section, we drive the adjoint equations and its boundary conditions for inverse design problem.

After calculation of the gradient vector, we can change the design variables using an optimization algorithm. In this work, steepest descent algorithm and smoothed steepest descent algorithm have been adapted to treat the design variables towards optimum values. In the steepest descent algorithm, the design variables vector x can be updated as:

$$x^{n+1} - x^n = -\alpha \nabla f \tag{43}$$

where α is the step length and ∇f is gradient vector of the cost function. In the smoothed steepest descent algorithm, the design variables vector x can be updated as:

$$\delta x = -\alpha \overline{\nabla} f \tag{44}$$

We replace the gradient ∇f by a smoothed value $\overline{\nabla} f$. To apply smoothing in the x direction, the smoothed gradient $\overline{\nabla} f$ may be calculated using a discrete approximation such as:

$$\overline{\nabla} f - \frac{\partial}{\partial \xi} \varepsilon \frac{\partial}{\partial \xi} \overline{\nabla} f = \nabla f \tag{45}$$

where ε is the smoothing parameter. The smoothing ensures that each new shape in the optimization process remains smooth. Consequently it is necessary to smooth the gradient vector when we apply surface points as design variables. The smoothing also allows us to use much larger steps, and leads to a large reduction in the number of design iterations.

Grid Modification

Jameson (1988) introduced a grid perturbation method that modifies the current location of the grid points based on perturbations at the surface geometry. The approach is not dependent on the method of structured grid generation. This method was also successfully used by Burgreen and Baysal (1994). In this method, the grid points are modified along each grid index line projecting from the surface. At first, the arc length between the surface point and the far-field point along the grid line is computed and then the grid points at each location along the grid line are attenuated proportional to its arc length distance from the surface point and the total arc length between the surface and the far-field. The algorithm can be described as:

$$\begin{cases} x_{i,j}^{new} = x_{i,j}^{old} + C_j (x_{i,1}^{new} - x_{i,1}^{old}) \\ \qquad\qquad j = 2, ..., j_{\max} \\ y_{i,j}^{new} = y_{i,j}^{old} + C_j (y_{i,1}^{new} - y_{i,1}^{old}) \end{cases} \tag{46}$$

where i is the current grid index. The vector C_j can be defined as:

$$C_j = 1 - (3 - 2N_j) N_j^2 \tag{47}$$

where N_j is the ratio of the arc length from the surface to the current grid point and the total arc length from the surface to the far-field along the grid line that can be written as:

$$N_j = \frac{\sum_{\ell=2}^{j} \sqrt{(x_{i,\ell} - x_{i,\ell-1})^2 + (y_{i,\ell} - y_{i,\ell-1})^2}}{\sum_{\ell=2}^{j\max} \sqrt{(x_{i,\ell} - x_{i,\ell-1})^2 + (y_{i,\ell} - y_{i,\ell-1})^2}} \tag{48}$$

Cost Function and Design Variables

The choice of design variables is one of the most crucial steps in any optimization procedure. The success of the optimization of the model problem depends on both the choice of design variables and the cost function.

A. Cost Function

The cost function for the inverse design problem in computational domain is defined as Eq. (19). The cost function for the drag minimization problem in computational domain is defined as:

$$C_d = \frac{-2}{\gamma p_\infty M_\infty^2 c} \int_{Bw} p (S_{21} \cos\alpha + S_{22} \sin\alpha)\, d\xi \tag{49}$$

B. Design Variables

Three shape parameterization methods are studied for two-dimensional aerodynamic shape optimization. They are the surface points, the definition of the NACA 4-digit airfoil series and the Hicks-Henne bump functions.

B.1. Surface Point

This method uses the mesh points to represent the surface. In other words, the design variables are the x and y locations of the mesh points. The main advantage of parameterizing a shape with surface points is that there is no restriction on the attainable geometry. Also, this parameterization technique can be easily implemented in any design problem. However, the use of surface points does present some difficulties. First, the independent displacement of a single point may cause the flow solver to become ill-conditioned, but more importantly it violates the assumption that the geometry surface is continuous. The point-wise gradients may contain high frequency modes, ultimately leading to unsmooth geometry profiles. Second, for complete aircraft configurations the surface point approach would require a very large number of design variables. This large number of design variables would limit the use of descent algorithms such as quasi-Newton approaches because of the high cost of the associated matrix operations.

B.2. Definition of the NACA 4-Digit Airfoil Series

In NACA 4-digit airfoil series, three parameters, m (the maximum mean camber), p (the chordwise position of the maximum mean camber) and t (maximum thickness of the airfoil) are used to define the airfoil shape. The NACA airfoils are constructed by combining a thickness envelope with a camber or mean line. The equations, which describe this procedure are:

$$\begin{aligned} x_u &= x - y_t(x) \sin\theta \\ y_u &= y_c(x) + y_t(x) \cos\theta \end{aligned} \tag{50}$$

and

$$\begin{aligned} x_l &= x - y_t(x) \sin\theta \\ y_l &= y_c(x) + y_t(x) \cos\theta \end{aligned} \tag{51}$$

where $y_t(x)$ is the thickness function, $y_c(x)$ is the camber line function, and

$$\theta = Arc\tan\left(\frac{dy_c}{dx}\right) \tag{52}$$

is the camber line slope. It is not unusual to neglect the camber line slope, which simplifies the equations and makes the reverse problem of extracting the thickness envelope and mean line for a given airfoil straightforward. The NACA 4-digit thickness distribution is given by:

$$\begin{aligned} \pm y_t = \frac{t}{0.2} (&0.29690\sqrt{x} - 0.126x - 0.3516x^2 \\ &+ 0.2843x^3 - 0.1015x^4) \end{aligned} \tag{53}$$

The camber line is given by:

$$y_c = \begin{cases} \dfrac{m}{p^2}(2px - x^2) & x \le p \\ \dfrac{m}{p-1}(1 - 2p + 2px - x^2) & x \ge p \end{cases} \tag{54}$$

The camber line slope is found from Eq. (52) using Eq. (54), and the upper and lower surface ordinates resulting from the combination of thickness and camber are then computed using Eqs. (50) and (51).

In present work m, t are taken as design variables and p is assumed to be 0.4.

B.3 Hicks-Henne "Bump" Functions

An alternative shape parameterization technique was proposed by Hicks and Henne (1974, 1978). They proposed the use of a set of smooth functions to perturb the initial geometry. The geometry can be parameterized using the weighted sum of a number of Hicks and Henne sine "bump" functions, as shown in Eq. (55)

$$y = y_{basis} + \sum_{j=1}^{N} \alpha_j f_j(x) \tag{55}$$

$$f_j(x) = \left[\sin\left(\pi x^{\frac{\log 0.5}{\log t_1}} \right) \right]^{t_2}, 0 \le x \le 1 \tag{56}$$

where t_1 locates the maximum point of the bump and t_2 controls the width of the bump. The design variables are the coefficients α_j multiplying the various Hicks-Henne bump functions. Figure 1 shows a set of 16 Hicks-Henne bump functions with parameter $t_2 = 10$.

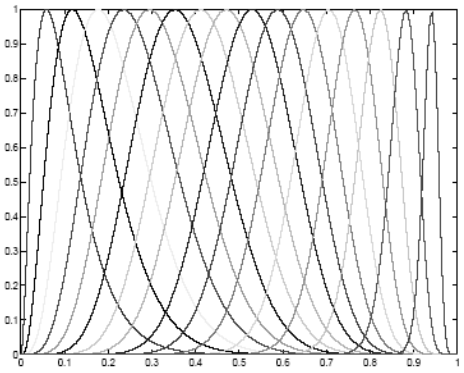

Figure 1. A set of 16 Hicks-Henne bump functions.

The different Hicks and Henne functions can be chosen such that only specific regions are refined, while the rest of the object to be optimized remains virtually undisturbed. The main result is that fewer design variables are needed to provide an adequate design space. Another advantage compared to the mesh point approach is the fact that the computed gradient always remains smooth and therefore, no smoothing of the gradient is required. This ensures that the successive surface shapes remain smooth. The disadvantage of the Hicks-Henne functions is that they are not orthogonal and they are unable to represent the complete set of continuous functions that vanish at $x = 0$ and $x = 1$. Thus, they do not guarantee that a solution, for example, of the inverse problem for a certain target pressure distribution will necessarily be attained.

Computational Cost of the Adjoint Method

Traditionally, finite-difference methods have been used to calculate sensitivities of aerodynamic cost functions. The computational cost of the finite-difference method for problems involving large numbers of design variables is both unaffordable and prone to subtractive cancellation error. In order to produce an accurate finite difference gradient, a range of step sizes must be used, and thus the ultimate cost of producing N gradient evaluations with the finite-difference method is the product mN, where m is the number of different step sizes used to obtain a converged finite difference gradient. (The used number of flow solvers is equal to mN). An estimate of the first derivative of a cost function is as:

$$\frac{\partial I}{\partial x} \approx \frac{I(x+h) - I(x)}{h} + O(h) \tag{57}$$

where h is the step size. A small step size is desired to reduce the truncation error $O(h)$, but a very small step size would also increase subtractive cancellation errors. But, in the adjoint method, according to Eq. (8) or Eq. (37), we can compute the gradient vector only with one flow solution in addition to one adjoint solution in each design cycle. The advantage is that Eq. (8) or Eq. (37) is independent of δw, with the result that the gradient of I with respect to an arbitrary number of design variables can be determined without the need for additional flow-field evaluations.

Since the cost of the adjoint approach is independent of the number of design variables, it is feasible to use the surface points as design variables, whereas the cost would be prohibitive, if the gradients were computed by the traditional finite difference method.

Outline of Design Procedure

Figure 2 is a graphical representation of the design procedure using adjoint method in present work.

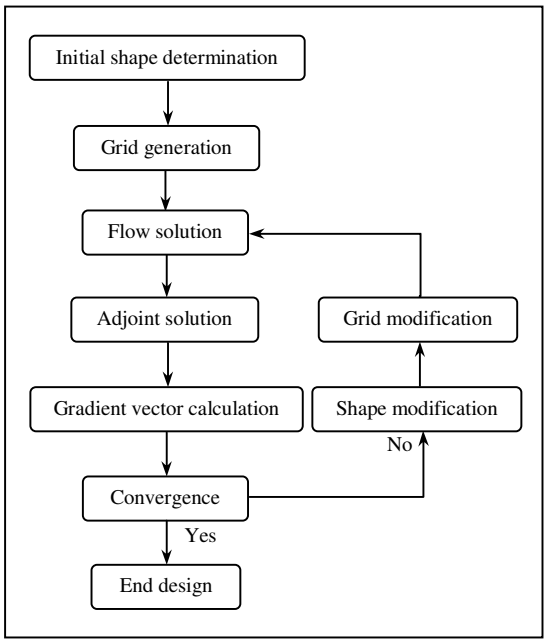

Figure 2. Design cycle.

Optimization Results

A. Inverse Pressure Design Problem

In this test case, NACA4415 is designed from NACA1410 airfoil. The flow is subsonic with Mach number of 0.65. Both the initial and target airfoils are at zero degree angle of attack. Surface points, parameters of the NACA 4-digit airfoil series (Airfoil

camber (m) and its thickness (t)) and the Hicks-Henne bump functions are used as the design variables. A 160 x 80 cells O-Type grid is employed in this calculation. The initial value for m, t are 0.01, 0.1 and the target value are 0.04, 0.15. The value of the parameter t_2 which controls the width of the Hicks-Henne bump functions was set to values of 30 and 32 bump functions for all the test cases.

Figure 3 compares the final airfoil shape after 85 design cycles for first method (surface points), second approach (parameters of the NACA 4-digit airfoil series) and third approach (Hicks-Henne bump functions). The gradient in first and third approaches is smoothed and the smoothed steepest descent algorithm acts as a preconditioner effectively reducing the number design cycles required to achieve a converged solution. The figure illustrates that all of the approaches achieve the final shape airfoil with a high degree of accuracy after 85 design cycles. Figure 4 shows the differences for the first 60% of the upper surface. The point-to-point match between the target airfoil and the first approach as well as the second and third approaches is clearly visible.

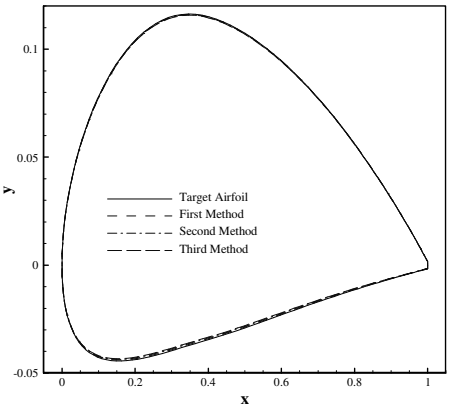

Figure 3. Comparison of final airfoils shapes for the inverse design problem.

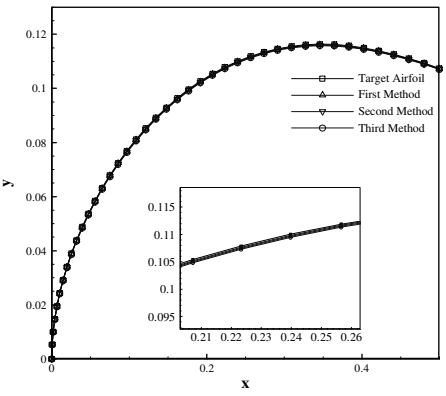

Figure 4. Comparison of final airfoils shapes at the leading edge for the inverse design problem.

Figure 5 shows convergence history of the norm of cost function gradient. The figure demonstrates that with using of third method, the convergence of the objective function drops 5 orders of magnitude to a level of 2.573E-07 for the second method and as low as 1.564E-07 with using of second method. The negative slope of the convergence plot indicates that a further drop in the objective function is still possible. The case with meshes points (first method) as the design variable attained a convergence level of 1.993E-07. This figure validates the convergence of optimization program. Figure 6 compares the final pressure distribution for the various cases against the target pressure. However, a slight discrepancy is observed at the shock, as shown by the inset in Fig. 6. The figure demonstrates the effectiveness of the mesh points, parameters of the NACA 4-digit airfoil series and Hicks-Henne bump functions that accurately capture the geometry of the NACA4415 airfoil.

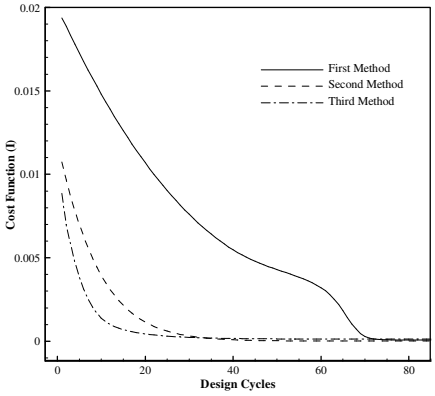

Figure 5. Convergence history of the norm of cost function gradient for the inverse design problem.

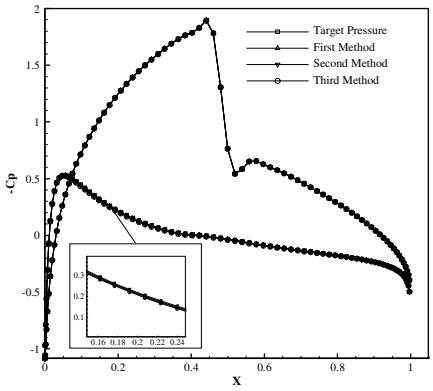

Figure 6. Comparison of final pressure distributions for inverse design problem.

B. Drag Minimization Problem

In this case, we have implemented the method in the constrained drag minimization. To evaluate the performance of the adjoint method in design problems with numerous design variables and also to evaluate the effects of the adoption of the design vector on the optimization results, the constrained drag minimization is performed using two different design vectors. In first test case, the surface points are used as the design variables and, in the second test case, m and t are adopted as design variables. The design is started by a NACA0012 airfoil at 3.0 degrees angle of attack. The flow is transonic with Mach number of 0.75. We performed computations on a 160 x 80 O-grid.

It is noticeable that the optimization has been performed in an inviscid and compressible transonic flow filed. Therefore, drag force is type of wave drag and is due to the produced shock wave on the surface (due to compressible effects).

B.1. Optimization Using the Surface Points (Test Case I)

Table 1 represents the design results. The reduction in the drag coefficient is considerable. We obtained 80.7 percent reduction in drag coefficient, but lift coefficient variations is very small.

Table 1. Design results.

	C_d	C_l	α
Initial	0.0317	0.6027	3
Optimal	0.0062	0.5937	1.17

Figure 7 represents the convergence of the cost function. This figure shows that full convergence of aerodynamic optimization is obtained after 260 design iterations and we reach to the optimum design. And 49.65 percent reduction in drag coefficient was obtained after 30 design cycles. Note that during 120 final cycles obtained only 1.74 percents reduction.

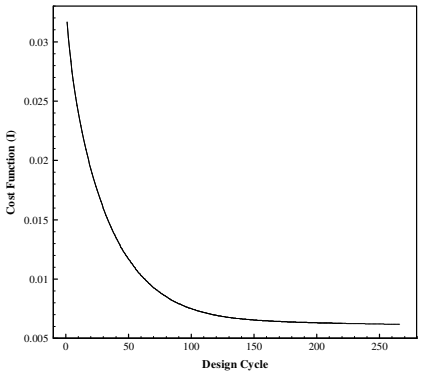

Figure 7. Convergence history of the cost function for the constrained drag minimization problem.

Figure 8 shows the convergence history of the norm of gradient during the design process. According to this figure, the trend is similar to that of the cost function variations. This figure validates the convergence of optimization program.

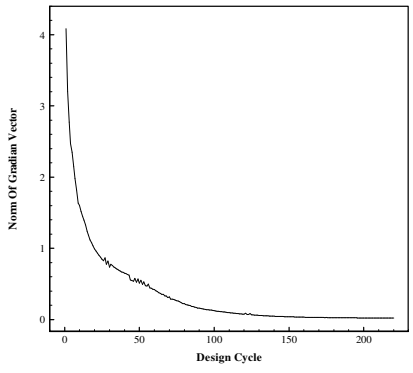

Figure 8. Convergence history of the norm of the gradient vector for the constrained drag minimization problem.

Figure 9 compares the initial and optimal pressure contours. Figure 10 represents the initial and optimal pressure coefficients. The figure shows that the strong shock on the initial airfoil surface has been weakened strongly and drag coefficient has been reduced but the surface area under the curve, which is represented the value of the lift coefficient, has remained constant and consequently this coefficient is nearly the same for both the initial and optimal airfoils.

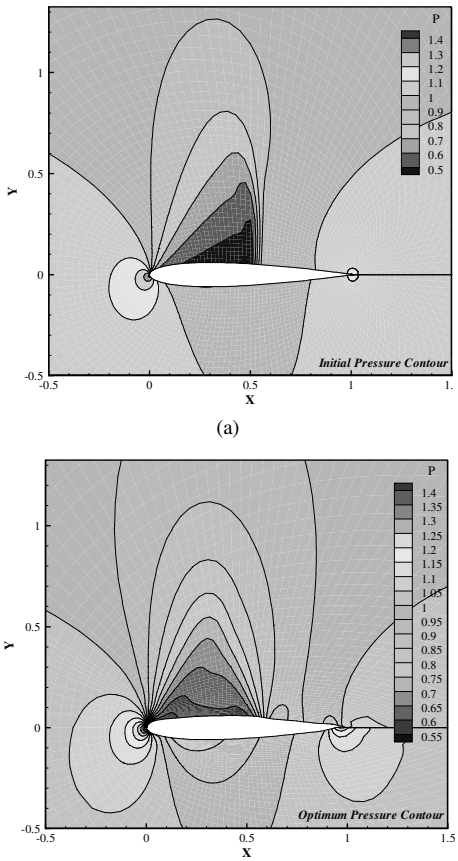

(a)

(b)

Figure 9. Pressure distribution contours for the constrained drag minimization problem. (a) Initial and (b) optimal.

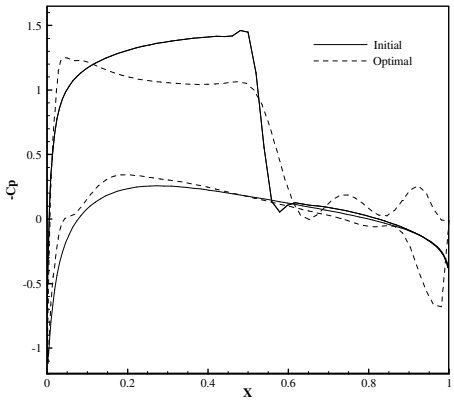

Figure 10. Comparison of pressure coefficient of NACA0012 and optimal airfoils for the constrained drag minimization problem.

Figure 11 shows the geometry of initial and optimal airfoils. The change in the upper surface and around the trailing edge is considerable, whereas the change in the lower surface is very small. Figures 10 and 11 show that the upper surface of the optimal airfoil has approached to a flat geometry. The flat surface has weakened the strength of the shock wave. Furthermore, the geometry of the airfoil at its trailing edge has curved downward to compensate the reduction of the lift coefficient due to the weakening the strength of the shock. It should be noted that for purpose of fixing the lift coefficient, the angle of attack is considered as an extra design variable.

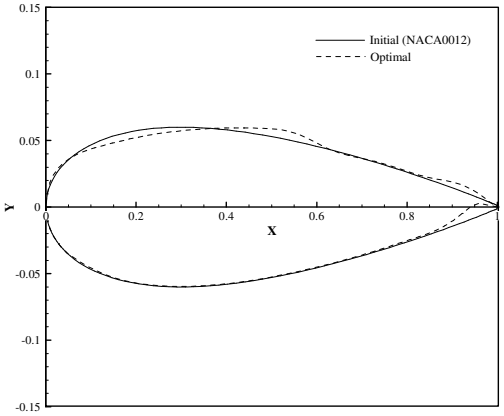

Figure 11. Comparison of NACA0012 airfoil and optimal airfoil for the constrained drag minimization problem.

B.2. Optimization Using the Relations of the Naca 4-Digit Airfoil Series (Test Case II)

Table 2 represents the design results. The reduction in the drag coefficient is considerable. We obtained 83.28 percent reduction in drag coefficient, but lift coefficient variations is very small (0.4 percents).

Table 2. Design results.

	m	t	C_d	C_l	α
Initial	0.00	0.12	0.0317	0.6027	3
Optimal	0.01072	0.0501	0.0053	0.6003	2.24

Figure 12 gives the variation of the cost function with design cycle. For this problem, the design cycle has 170 iterations. The drag coefficient reduction is 81.92 percent during the first 80 design cycles. This coefficient has only 1.36 percent reduction in the last 90 cycles. Figure 13 shows the variation of the norm of the gradient vector with design cycle. The trend is similar to that of the cost function. With regard to Figs. 12 and 13, the convergence of the optimization program is evident.

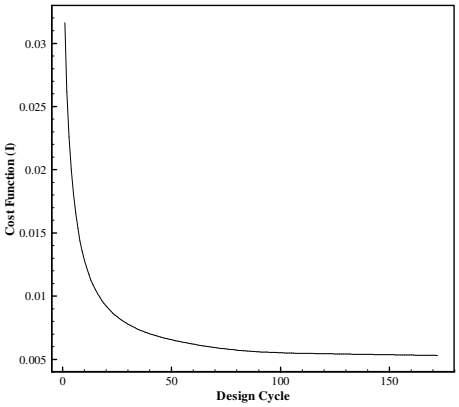

Figure 12. Convergence history of the cost function for the constrained drag minimization problem.

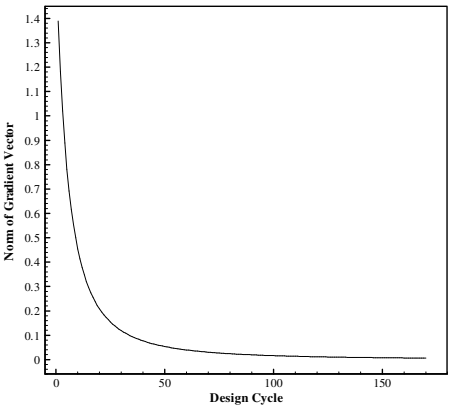

Figure 13. Convergence history of the norm of the gradient for the constrained drag minimization problem.

Figure 14 shows the pressure contours around the initial and optimal airfoils. Regarding this figure, the shock wave has moved toward the leading edge and its strength is considerably reduced. Figure 15 gives the pressure coefficients on upper and lower surface of initial and optimal airfoils. It is seen that the location of the shock wave has changed and its strength is reduced. But the surface under the curve is remained constant, which reveals no change in lift coefficient. It is clear that the drag coefficient reduction has been achieved due to reduction of thickness, whereas increase of the camber has led to increase of the lift coefficient. In fact, the reduction of the lift due to the reduction of the thickness has been compensated by increase of the camber. More over the variation of the angle of attack is such that the lift coefficient remains constant.

It should be noted that the convergence rate of the optimization program is strongly dependent on the step size of α in optimization algorithm. If the step size was taken larger, it increased the convergence rate. But adoption of a larger step size for α leads to increase in geometry parameters and decrease in accuracy of the calculated gradients. Sometimes, larger step size caused oscillatory behavior of the gradients. More over adoption of smaller step size for α led to increase in number of design cycles.

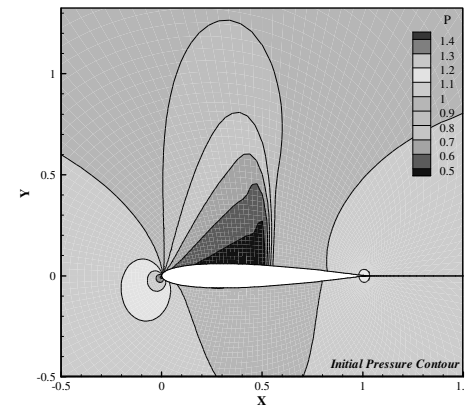

(a)

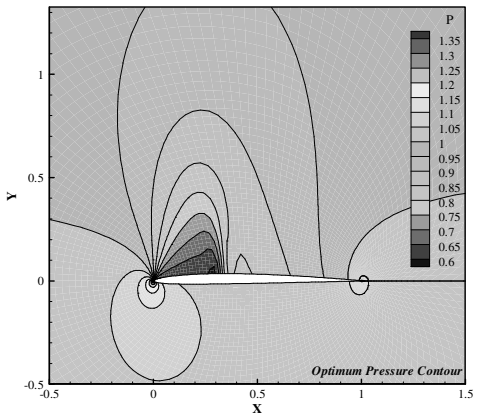

(b)

Figure 14. Pressure distribution contours for the constrained drag minimization problem. (a) Initial and (b) optimal.

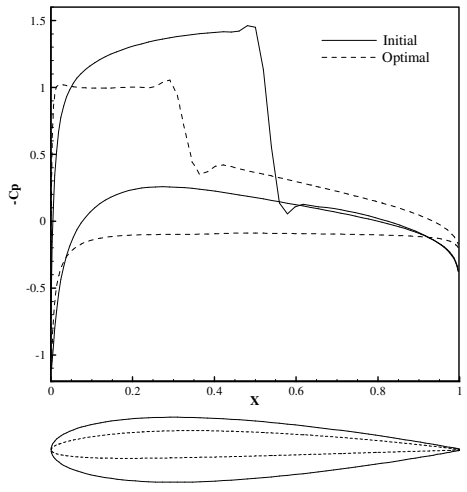

Figure 15. Comparison of pressure coefficient and geometry of NACA0012 and optimal airfoils for the constrained drag minimization problem.

It is known that the location and strength of a shock wave in transonic regime are main parameters in drag calculation. Comparison of results of the optimization problem using two different design vectors – in one of them the surface points are considered as design variables and in the other one the parameters of 4-digit NACA airfoil are design variables (Figs. 9 and 14 or Figs. 10 and 15) – shows that when the surface points of the airfoil are design variables, the upper surface geometry changes such that the strength of the shock wave is reduced, but the location of the shock wave has no change. In fact, the drag reduction is carried out via the variation of the curvature only at region of the shock wave. And the lift coefficient is recovered via the increase in curvature only at the trailing edge region. When the thickness and camber of NACA four digits were considered as design variables, the shock wave moves toward the leading edge and the strength is reduced. In fact, the drag reduction is carried out via reduction of the thickness on all of the surface points and recovery of the lift coefficient is achieved by increasing the camber on all of the surface points.

Table 3 summarizes the required runtime and number of adjoint and flow solvers to achieve the convergence of the optimization program for the constrained drag minimization problem. The used computer specification is "Intel(R) Core(TM) Due CPU T2450@ 2.00GHz, 1GB of RAM".

Table 3. Runtime and number of adjoint and flow solvers of the drag minimization problem.

	Runtime	Number of adjoint solvers	Number of flow solvers	Number of design cycles
Test case I	504 minutes	440	220	220
Test case II	425 minutes	340	170	170

Conclusions

In this paper, we implemented the adjoint equations method for the inverse pressure design and the constrained drag minimization problems. In the inverse design problem, surface points, parameters of the NACA 4-digit airfoil series (Airfoil camber (m) and its thickness (t)) and the Hicks-Henne bump functions are used as the design variables. In this problem, values of design variables were obtained successfully. The results of the test case show that we can use the adjoint approach as an efficient tool in airfoil inverse design problem. To evaluate the performance of the adjoint method in design problems with numerous design variables and also to evaluate the effects of the adoption of the design vector on the optimization results in the drag minimization problem, the minimization was performed using two different design vectors. It was shown that the mechanism and the trend of drag reduction during the optimization process were strongly affected by the type of design vector. By using the adjoint equations method, we can design high lift or low drag airfoils according to the desired surface pressure.

References

Amoignon, O., 2004, "Adjoint-Based Aerodynamic Shape Optimization", Ph.D. Thesis, Uppsala University, Sweden.

Baysal, O. and Ghayour, K., 2001, "Continuous adjoint sensitivities for optimization with general cost functional on unstructured meshes", *Journal of AIAA*, Vol. 39, No. 1, pp. 48-55.

Burgreen, G.W., Baysal, O., 1994, "Three-dimensional aerodynamic shape optimization of wings using sensitivity analysis", AIAA paper 94-0094, 32nd Aerospace Sciences Meeting and Exhibit, Reno, Nevada.

Dadone, A. and Grossman, B., 2000, "Progressive optimization of inverse fluid dynamic design problems", *Journal of Computers & Fluids*, Vol. 29, No. 2000, pp. 1-32.

Dwight, R.P. and Brezillon, J., 2006, "Effect of various approximations of the discrete adjoint on gradient-based optimization", 44th AIAA Aerospace Sciences Meeting and Exhibit Conference, Reno Nevada.

Elliott, J. and Peraire, J., 1997, "3-D aerodynamic optimization on unstructured meshes with viscous effects", AIAA paper 97-1849, 35th Aerospace Sciences Meeting and Exhibit, Reno, Nevada.

Gauger, N.R. and Brezillon, J., 2002, "Aerodynamic shape optimization using adjoint method", *Journal of Aero. Soc. of India*, Vol. 54, No. 3, pp. 110-121.

Hazra, S.B., 2004, "An efficient method for aerodynamic shape optimization", 10th AIAA/ISSMO Multidisciplinary Analysis and Optimization Conference, New York, USA.

Hicks, R.M. and Henne., P.A., 1978, "Wing design by numerical optimization", *J. of Aircraft*, Vol.15, pp. 407-412.

Hicks, R.M., Murman, E.M. and Vanderplaats, G.N., 1974, "An assessment of airfoil design by numerical optimization", NASA TM X-3092, Ames Research Center, Moffett Field, California.

Jameson, A., 1988, "Aerodynamic design via control theory", *Journal of Scientific Computing*, Vol. 3, No. 3, pp. 233-260.

Jameson, A. and Alonso, J., 1996, "Automatic aerodynamic optimization on distributed memory architectures", AIAA paper 96-0409, 34th Aerospace Sciences Meeting and Exhibit, Reno, Nevada.

Jameson, A., 1997, "Re-engineering the design process through computation", AIAA paper 97-0641, 35th Aerospace Sciences Meeting and Exhibit, Reno, Nevada.

Jameson, A., Schmidt, W. and Turkel, E., 1981, "Numerical solutions of the Euler equations by finite volume methods with Runge-Kutta time stepping schemes", AIAA paper 81-1259.

Michieli Vitturia and M., Beuxb, M.F., 2006, "A discrete gradient-based approach for aerodynamic shape optimization in turbulent viscous flow", *Journal of Finite Elements in Analysis and Design*, Vol. 5, No. 12, pp. 187-202.

Nadarajah, S. and Jameson, A., 2000, "A comparison of the continuous and discrete adjoint approach to automatic aerodynamic optimization", AIAA paper 2000-0667, 38th Aerospace Sciences Meeting and Exhibit, Reno, Nevada.

Nadarajah, S. and Jameson, A., 2001, "Studies of the continuous and discrete adjoint approaches to viscous automatic aerodynamic shape optimization", AIAA paper 2001-2530, 15th Computational Fluid Dynamics Conference, Anaheim.

Nadarajah, S., 2003, "The Discrete Adjoint Approach to Aerodynamic Shape Optimization", Ph.D. Thesis, Stanford University, Stanford, USA.

Pironneau, O., 1984, "Optimal Shape design for Elliptic Systems", Springer-Verlag, New York.

Qiao, Z.D., Yang, X.D., Qin, X.L. and Zhu, B., 2002, "Numerical optimization design by solving adjoint equations", ICAS Congress.

Xie, L., 2002, "Gradient-Based Optimum Aerodynamic Design Using Adjoint Methods", Ph.D. Thesis, Virginia Polytechnic Institute and State University, Virginia, USA.